# Joint source-channel fractal image coding with unequal error protection

Youssef Charfi, charfi@fmi.uni-konstanz.de, ph. (+49) 7531 88-2200
Vladimir Stanković, stankovi@fmi.uni-konstanz.de, ph. (+49) 7531 88-3020
**Corresponding author:**
Raouf Hamzaoui, hamzaoui@fmi.uni-konstanz.de, ph. (+49) 7531 88-4579
Ameur Haouari, haouari@fsr.ac.ma, ph. (+212)37-778973
Dietmar Saupe, saupe@fmi.uni-konstanz.de, ph. (+49) 7531 88-4433

*Address/fax of authors Charfi, Stanković, Hamzaoui, Saupe:*
University of Constance, Department of Computer and Information Science
Fach D 67, 78457 Konstanz, Germany
FAX: (+49) 7531 88-3577
*Address/fax of A. Haouari:*
University Mohammed V, LEESA, Faculty of Science
B.P. 1014, Rabat, Morocco
FAX: (212)7-778973

May 8, 2002

**Abstract**

We propose a joint source-channel coding system for fractal image compression. We allocate the available total bit rate between the source code and the channel code using a Lagrange multiplier optimization technique. The principle of the proposed unequal error protection strategy is to partition the information bits into sensitivity classes and to assign one code from a range of error-correcting codes to each sensitivity class in a nearly optimal way. Experimental results show that joint source-channel coding with fractal image compression is feasible, leads to efficient protection strategies, and outperforms previous works in this field that only covered channel coding with a fixed source rate.

**Keywords:** fractal image compression, joint source-channel coding, unequal error protection.

# 1 Introduction

Robust and efficient transmission of images over noisy channels has recently attracted a widespread interest because of the increasing popularity of the Internet and wireless multimedia devices and services. According to Shannon's separation theorem, the source coder and the channel coder may be designed independently [1]. However, the theorem holds under asymptotic assumptions which are not fulfilled in practice [2]. This motivates the design of joint source-channel coders. Efficient solutions for the allocation of the total transmission rate between the source coder and the channel coder were proposed for many compression systems, including vector quantizers, discrete cosine transform and wavelet-based coders [3, 4, 5, 6, 7]. In this paper, we consider the problem of joint source-channel coding for fractal image compression. Because the bits of the fractal code have unequal importance we take into account unequal error protection techniques. Rate-distortion optimization is applied to the source and all parts of the channel code.

Fractal image compression provides satisfactory rate-distortion results, fast decoding, and resolution independence [8]. A fractal code is a binary representation of a contractive image operator whose unique fixed point is close to the original image. The image operator is based on an image partition in blocks and an affine similarity between the blocks in the partition and other blocks from the same image. The decoder recovers the fixed point by iterating the image operator. Fractal codes are very sensitive to channel errors because errors propagate during the decoding. Although more than 650 papers have been

dedicated to fractal image compression [9], only a few considered transmission through noisy channels. The first work about error protection for fractal image codes is due to Streit and Hanzo [10]. The authors used a two-level error protection scheme with Bose-Chaudahuri-Hocquenghen (BCH) codes [11] to send a fractal code over a Rayleigh-fading channel. The authors observed that unequal error protection (UEP) has a significantly better performance than equal error protection (EEP). However, the proposed UEP scheme was given for a poor coder based on uniform partitions, and the unequal error protection was not optimized. Novak [12] introduced a model-residual fractal coder and showed that it is less sensitive to errors than a standard fractal coder. Error protection was not considered in this work. Noh, Kim, and Kim [13] used an interpolation technique for reconstructing blocks lost during the transmission of a fractal code in broadband integrated-services digital networks with asynchronous transfer mode protocols. Finally, Stanković, Hamzaoui, and Saupe [14] proposed a rate-distortion based UEP technique for the allocation of the information bits into a set of protection classes. The goal of the algorithm is to minimize the expectation of the reconstruction error for a given bit error rate (BER) in a binary symmetric channel (BSC) and for a fixed source rate subject to a constraint on the number of protection bits. The performance of the system at a target transmission rate can be improved significantly by determining the optimal corresponding source rate. Unfortunately, the optimal tradeoff between the source rate and the channel rate is not obvious because of the great number of parameters in the fractal source coder and the UEP scheme.

This study continues and extends the discussion of [14]. We first introduce a UEP strategy for fractal image codes that improves the results of [14] without increasing the computing requirements. Then we provide techniques for joint source-channel coding yielding far superior results than those obtained with UEP for fixed source rates.

This paper is organized as follows. In Section 2, we describe a generic fractal coder. Our main contribution is Section 3, in which we present a fast unequal error protection technique and a joint source-channel coding system. We discuss the tradeoff between source and channel bit rates and provide an analysis of the sensitivity of the individual bits in the fixed length codewords of the fractal code, upon which we base a UEP scheme. Our method rapidly yields a suboptimal source-channel code pair whose performance is comparable to that of the corresponding full search solution. In Section 4, we give simulation results which show that our system outperforms all previous schemes where the source rate is

fixed and only the channel rate is optimized.

## 2 Fractal image coding

In fractal compression, the encoder finds a contractive image operator $T$ whose fixed point $f_T$ approximates the original image $f^*$. The decoder constructs $f_T$ as the limit of $\{f^{(k)}\}_{k\geq 0}$, where $f^{(k+1)} = T(f^{(k)})$ and $f^{(0)}$ is an arbitrary initial image. For example, in this paper the operator $T$ is given by a quadtree partition of the image support $\mathcal{I}$ into $n_R$ disjoint square blocks called *ranges* and by *fractal parameters* associated to each range $R_i$, $1 \leq i \leq n_R$, and consisting of

- a square block (*domain*) $D_{j_i}$ from $D_1, ..., D_{n_D} \subset \mathcal{I}$,
- an isometry of the square $I_{k_i} \in \{I_1, I_2, ..., I_8\}$,
- a *scaling factor* $s_{l_i} \in \{s_1, ..., s_{n_s}\} \subset (-1, 1)$,
- and an *offset* $o_{m_i} \in \{o_1, ..., o_{n_o}\} \subset \mathbb{R}$.

The parameters $D_{j_i}, I_{k_i}, s_{l_i}$, and $o_{m_i}$ are selected from their respective sets such that

$$\widehat{\mathbf{R}}_i = s_{l_i} I_{k_i} A_i \mathbf{D}_{j_i} + o_{m_i} \mathbf{1} \tag{1}$$

is the best $l_2$ approximation of $\mathbf{R}_i$. Here boldface capital letters like, e.g., $\mathbf{B}$ denote the array of pixel intensities of $f^*$ in the corresponding subset $B \subset \mathcal{I}$, the operator $A_i$ downsamples $\mathbf{D}_{j_i}$ via pixel averaging to match the range size, and $\mathbf{1}$ is the block with intensity 1 at every pixel.

We used Fisher's quadtree coder [8], which we modified according to Øien's orthogonalization technique [15]. Thus, the approximation (1) was replaced by

$$\widehat{\mathbf{R}}_i = s_{l_i} I_{k_i} A_i (\mathbf{D}_{j_i} - \mu(\mathbf{D}_{j_i})\mathbf{1}) + o_{m_i} \mathbf{1}. \tag{2}$$

Here $\mu(\cdot)$ denotes the mean of a block. This yields a more robust code because in contrast to equation (1), errors in the scaling factor do not affect the mean of a reconstructed block.

Using the method of least squares, the optimal nonquantized scaling factor and offset associated to a domain $D$ and an isometry $I$ are

$$\begin{aligned} s &= \frac{|R_i|\langle C, \mathbf{R}_i\rangle - |R_i|^2 \mu(\mathbf{D})\mu(\mathbf{R}_i)}{|R_i|\langle C, C\rangle - \mu(\mathbf{D})^2}, \\ o &= \mu(\mathbf{R}_i). \end{aligned}$$

Here $|R_i|$ is the number of pixels in $R_i$, $C = IA_i\mathbf{D}$, and $\langle \cdot, \cdot \rangle$ denotes the inner product. The error $\sum_{i=1}^{n_R} \|\mathbf{R}_i - \widehat{\mathbf{R}}_i\|_2^2$ is called *collage error*. The decoder constructs $f_T = \lim_{k\to\infty} f^{(k)}$ through

$$\mathbf{R}_i^{(k+1)} = s_{l_i} I_{k_i} A_i(\mathbf{D}_{j_i}^{(k)} - \mu(\mathbf{D}_{j_i}^{(k)})\mathbf{1}) + o_{m_i}\mathbf{1},\ 1 \le i \le n_R,$$

where $\mathbf{R}_i^{(k+1)}$ (respectively $\mathbf{D}_{j_i}^{(k)}$) is the array of pixel intensities of $f^{(k+1)}$ in $R_i$ (respectively of $f^{(k)}$ in $D_{j_i}$). The reconstruction error $d = \|f^* - f_T\|_2^2$ is called the *attractor error*.

The fractal code associated to $T$ consists of bits for the quadtree and a codeword for each range block $R$ in the partition. In the following, we use a set of $n_s = 2^5$ scaling factors and a set of $n_o = 2^7$ offsets. For each range, the candidate domains consist of blocks that are twice the range size and whose upper-left pixels are located at coordinates $(i, j)$, where $i \equiv 0 \pmod 4$ and $j \equiv 0 \pmod 4$. For an image of size 512 $\times$ 512 this leads to $n_D = 2^{14}$ domains. We denote the (binary) range codeword, consisting of 29 bits, by

$$\omega_R = s_4 \cdots s_0 o_6 \cdots o_0 i_2 \cdots i_0 d_{13} \cdots d_0. \tag{3}$$

In Fisher's original coder, if the optimal scaling factor for a range is equal to zero, then no domain and isometry bits are sent because they are redundant. For such a range, the corresponding codeword would comprise of less than 29 bits. However, to ensure synchronization in our transmission system, we must send bits for the zero scaling factor, an arbitrary isometry, and a domain block address. Thus, all codewords have a length of 29 bits.

# 3 Joint source-channel coding system

## 3.1 Tradeoff between source and channel rates

We consider the quadtree fractal coder of the previous section and assume that the header bits of the fractal code that include the definition of the quadtree image partition are perfectly protected. This is not a severe limitation since the header that constitutes less than 2/100 of the total code, can be perfectly protected with a negligible increase of the bit rate. Therefore we consider only unequal error protection of the $n_R$ codewords $\omega_{R_i}, i = 1, ..., n_R$, see (3).

We define a finite set of channel code rates $\mathcal{R} = \{r_1, ..., r_l\}$. For example, one can use a range of rate-compatible punctured convolutional (RCPC) code rates [16]. A code of a fractal transform $T$ is

protected by a strategy $S$ that assigns a code rate to each bit of $\omega_R$. We assume that all ranges are protected with the same strategy. We denote the set of possible strategies by $\Omega$ and the set of available fractal transforms by $\mathcal{T}$. These sets $\Omega$ and $\mathcal{T}$ are finite sets.

Suppose that the original image $f^*$ is encoded with a transform $T$ and protected with a strategy $S$. Let $S(T)$ be the transform obtained after channel decoding. Then $D(T,S) = E\{\|f^* - f_{S(T)}\|_2^2\}$ is the expected distortion due to both the source quantization and the channel noise. Let $R_s(T)$ be the source bit rate associated to $T$ and $R_c(T,S)$ be the channel bit rate associated to the protection of $T$ by $S$. An optimal joint source-channel coder finds a pair $(T^*, S^*)$ that solves the constrained minimization problem

$$\min_{(T,S)\in\mathcal{T}\times\Omega} D(T,S) \text{ subject to } R_s(T) + R_c(T,S) \leq R_t,$$

where $R_t$ is the available transmission rate. This constrained optimization problem can be simplified by converting it into the unconstrained problem

$$\min_{(T,S)\in\mathcal{T}\times\Omega} L(T,S,\lambda) \tag{4}$$

where

$$L(T,S,\lambda) = D(T,S) + \lambda(R_s(T) + R_c(T,S)) \tag{5}$$

and $\lambda \geq 0$ is a Lagrange multiplier [17]. In practice, we choose a set $\mathcal{T}$ of fractal transforms yielding image codes with differing source rates and minimize $L(T,S,\lambda)$ for each $T \in \mathcal{T}$,

$$\min_{T\in\mathcal{T}} \left[\min_{S\in\Omega} L(T,S,\lambda)\right]. \tag{6}$$

Let us call this optimization *Algorithm JSCC-0*. To meet the constraint on the total rate, the bisection method can be applied requiring that the optimization be done for several values of the Lagrange multiplier $\lambda$.

By separating the two nested minimizations in (6), we obtain an algorithm that is faster than JSCC-0 but sacrifices some quality for the sake of speed. For initialization, we choose a medium strength equal error protection strategy, $S_0 = (r_{\lfloor l/2 \rfloor}, ..., r_{\lfloor l/2 \rfloor})$. Then a sequence of pairs $(T_k, S_k)_{k=1,...,k_{\max}}$ is obtained in $k_{\max}$ iterations as follows,

$$T_k = \arg\min_{T\in\mathcal{T}} L(T, S_{k-1}, \lambda), \tag{7}$$

$$S_k = \arg\min_{S\in\Omega} L(T_k, S, \lambda). \tag{8}$$

As final result we obtain the transform $T_{k_{\max}}$, the strategy $S_{k_{\max}}$, and the associated Lagrangian cost $L(T_{k_{\max}}, S_{k_{\max}}, \lambda)$. Let us call this modified procedure *Algorithm JSCC-1.*

Let $(T_k, S_k)_{k=1,2,\ldots}$ be the sequence of fractal transforms and protection strategies produced in Algorithm JSCC-1. Then the sequence $L(T_k, S_k, \lambda)_{k=1,2,\ldots}$ is monotonically decreasing.

The computing times are dominated by $t_D$, the simulation time required to evaluate the total distortion for a choice of $(T, S, \lambda)$. For JSCC-0 this amounts to a total time of $|\mathcal{T}|t_D$ and for JSCC-1 this is $k_{\max}t_D$.

After the next subsection on bit sensitivity analysis, we discuss the minimization of the Lagrangian cost $L(T, S, \lambda)$ for a fixed transform $T$ which is required in (8). We will arrive at three unequal error protection algorithms with different qualities and complexities, which we call *Algorithms UEP-0, UEP-1,* and *UEP-2* all of which can be combined with JSCC-0 and JSCC-1.

## 3.2 Bit sensitivity analysis

The importance of the bits of the range codewords $\omega_{R_i}$, $i = 1, \ldots, n_R$ can be determined by corrupting the bits at the same position in a codeword with a certain bit error rate and computing the degradation of the peak-signal-to-noise ratio (PSNR) in the reconstructed image. Figure 1 shows the resulting PSNR degradations for the $512 \times 512$ Lenna image at source rate 0.21 bpp and a binary symmetric channel bit error rate (BER) of $10^{-1}$. Each PSNR is averaged over 50 experiments with the same BER. The figure shows that the codeword bits have unequal importance. Moreover, for the offset and the scaling factor, a more significant bit of a given parameter was more sensitive than a less significant bit. For the domain, all bits except for the two least significant ones had about the same sensitivity. This was expected because for the used domain pool an error in the two least significant bits selects a domain that overlaps the original one, whereas an error in any of the other bits selects an unrelated domain. We obtained similar results for other BERs and other images at several source rates.

Figure 2 shows the PSNR reconstruction quality as a function of the BER when *all* the bits of only one fractal parameter (offset, scaling, isometry, domain address) were corrupted. Again, each PSNR value is averaged over 50 experiments with the same BER. The analysis shows that the different fractal parameters had unequal importance. The most sensitive parameter was the offset, followed by the domain, the isometry, and the scaling factor.

Each of the 29 bits in the codewords $\omega_{R_i}$ may be protected using a different channel code rate. To

reduce the complexity of the optimization we suggest to partition the 29 codeword bits into $m \leq 29$ sensitivity classes $C_1, ..., C_m$ and to protect all bits in a class $C_k$ with the same channel rate $r_{j_k} \in \mathcal{R}$. The partition of the bits into the classes is based on the importance of the bits. This was done by clustering the 29 codeword bits into $m$ sets with the k-means algorithm applied to the set of 29 values of PSNR degradation shown in Figure 1. The result for $m = 13$ is given in Table 1.

### 3.3 Unequal error protection of fractal image codes

Our goal is to compute $\min_{S \in \Omega} L(T, S, \lambda)$ for fixed $T \in \mathcal{T}$ and $\lambda \geq 0$. Throughout this paper, we assume that the used error protection scheme has the property that increasing the number of protection bits increases the correction capability. In other words, the residual bit error rate is assumed to be a monotonically increasing function of the code rate.

In this subsection, we present three methods for unequal error protection of fractal codes, in which codeword bits from the same class $C_k$ are equally protected. The channel bit rate $R_c(T, S)$ is given by

$$R_c(T, S) = n_R \sum_{k=1}^{m} \left( \frac{1 - r_{j_k}}{r_{j_k}} \right) n_k, \tag{9}$$

where $n_R$ denotes the number of range blocks of the image. For $k = 1, ..., m$, the number of bits of a range codeword assigned to the sensitivity class $C_k$ is $n_k$. These bits are protected by the same code rate $r_{j_k}$ in all codewords.

For $k = 1, 2, \ldots, m-1$, the bits in class $C_k$ are more sensitive to channel errors than the bits in class $C_{k+1}$. Thus, it is reasonable to use a protection strategy such that $r_{j_k} \leq r_{j_{k+1}}$. With this convention we give the following definition.

**Definition 1** *Let $\mathcal{R} = \{r_1, ..., r_l\}$ be the set of channel code rates. The set $\Omega$ of protection strategies is*

$$\Omega = \{(r_{j_1}, r_{j_2}, ..., r_{j_m}) \in \mathcal{R}^m \mid r_{j_1} \leq r_{j_2} \leq ... \leq r_{j_m}\}.$$

For convenience, let us order the rates in $\mathcal{R}$ to be increasing, $r_1 < r_2 < \cdots < r_l$. Thus, the set $\Omega$ of protection strategies is

$$\Omega = \{(r_{j_1}, ..., r_{j_m}) \in \mathcal{R}^m \mid j_1 \leq j_2 \leq ... \leq j_m\}.$$

The requirement of increasing code rates in a strategy $S \in \Omega$ reduces the size of the space $\mathcal{R}^m$ of strategies from $l^m$ to $f(m, l) = \binom{m+l-1}{m}$, as shown by the next lemma. Although $f(m, l)$ is still of order $l^m$ the

reduction of size is relevant in practice. For the example of $m = 13$ and $l = 6$, a practical setting used in our experiments, $f(m,l) = 8568$, which is less than a millionth of $l^m = 6^{13}$.

**Lemma 1** *Let $A = \{1, 2, ..., l\}$. The number of $m$-tuples $(j_1, ..., j_m) \in A^m$ with $j_1 \leq \cdots \leq j_m$ is $f(m,l) = \binom{m+l-1}{m}$.*

**Proof** The proof is straightforward by induction on $m$ [14].

We call the minimization $\min_{S \in \Omega} L(T, S, \lambda)$ by enumeration of all $f(m,l)$ (increasing) channel code rate allocations *Algorithm UEP-0*.

We now propose to replace the enumeration in the minimization $\min_{S \in \Omega} L(T, S, \lambda)$ by a faster heuristic algorithm. For this purpose, we introduce more notations.

**Definition 2** *Let $m$ be the number of protection classes and $\mathcal{R} = \{r_1, ..., r_l\}$ be the set of channel code rates. For $K = 1, ..., m$ and $r_i \in \mathcal{R}$ the set of protection strategies in $\Omega$ which prescribe to protect the first $K$ classes $C_1, ..., C_K$ by the same rate $r_i$ and the remaining classes by higher rates is denoted by*

$$\Omega_K(r_i) = \{ \quad (r_{j_1}, ..., r_{j_m}) \in \Omega \mid$$
$$r_i = r_{j_1} = \cdots = r_{j_K} < r_{j_{K+1}} \leq \cdots \leq r_{j_m} \quad \}.$$

Since the channel code rates are ordered by increasing numbers, $\Omega_K(r_i)$ is the set of tuples $(r_{j_1}, ..., r_{j_m}) \in \Omega$ with

$$i = j_1 = \cdots = j_K < j_{K+1} \leq \cdots \leq j_m.$$

If we replace the strict inequality $r_{j_K} < r_{j_{K+1}}$ by $r_{j_K} \leq r_{j_{K+1}}$, we obtain the set of protection strategies in $\Omega$ which prescribe to protect the classes $C_1, ..., C_K$ by rate $r_i$. In other words, this set of strategies is

$$\overline{\Omega}_K(r_i) = \bigcup_{k=K,...,m} \Omega_k(r_i).$$

We note that the strategy sets $\Omega_K(r_i)$ as well as the sets $\overline{\Omega}_1(r_i)$ make up a partition of the set $\Omega$ of all allowed strategies.

**Lemma 2**

$$\Omega = \bigcup_{\substack{i=1,...,l \\ K=1,...,m}} \Omega_K(r_i) = \bigcup_{i=1,...,l} \overline{\Omega}_1(r_i)$$

*where $\Omega_K(r_i) \cap \Omega_{K'}(r_{i'}) = \emptyset$ if $K \neq K'$ or $i \neq i'$ and $\overline{\Omega}_1(r_i) \cap \overline{\Omega}_1(r_{i'}) = \emptyset$ if $i \neq i'$.*

Also note that $\Omega_K(r_l) = \emptyset$ for $K = 1, ..., m-1$. This means that if source code bits from the most sensitive class $C_1$ are protected by the weakest channel code, i.e., by the highest rate $r_l \in \mathcal{R}$, then all bits from the remaining classes $C_2, ..., C_m$ can only be protected by the same channel code rate.

For each protection strategy $S = (r_{j_1}, ..., r_{j_m}) \in \overline{\Omega}_K(r_i)$, $i = 2, ..., l$, $K = 1, ..., m$ we can define a successor strategy $\mathrm{succ}(S)$ by putting the next highest protection on the first $K$ classes, i.e., by replacing the rate $r_i$ of the first $K$ classes by the nearest lower rate $r_{i-1}$.

**Definition 3** *For $i = 2, ..., l$, $K = 1, ..., m$ and $S = (r_{j_1}, ..., r_{j_m}) = (r_i, ..., r_i, r_{j_{K+1}}, ..., r_{j_m}) \in \overline{\Omega}_K(r_i)$, let*

$$\mathrm{succ}(S) = (r_{i-1}, ..., r_{i-1}, r_{j_{K+1}}, ..., r_{j_m}) \in \Omega_K(r_{i-1}).$$

We remark that the successor function yields a bijection between the sets $\overline{\Omega}_K(r_i)$ and $\Omega_K(r_{i-1})$ for all $i = 2, ..., l$, $K = 1, ..., m$.

Let us consider two protection strategies $S', S'' \in \overline{\Omega}_K(r_i)$ with $i \geq 2$. *Then we may assume for the Lagrangian costs that $L(T, \mathrm{succ}(S'), \lambda) \geq L(T, \mathrm{succ}(S''), \lambda)$ if and only if $L(T, S', \lambda) \geq L(T, S'', \lambda)$.* In the successors only the first $K$ channel code rates $r_i$ are replaced by $r_{i-1}$. It is reasonable to assume that the expected distortion $D(T, S)$ is decreased by about the same amount in both cases. Since also the rate changes by an equal amount, we obtain our assumption. Our results in Section 4 empirically justify this assumption. If we consider a model in which distortion due to errors in different protection classes is additive, we can also prove our assumption.

**Lemma 3** *Assume there exist distortion functions $D_k^T(r)$ for $k = 1, ..., m$, $r \in \mathcal{R}$, and $T \in \mathcal{T}$, such that the total distortion can be written as*

$$D(T, S) = D(T, (r_{j_1}, ..., r_{j_m})) = \sum_{k=1}^{m} D_k^T(r_{j_k}).$$

*Then, for $K = 1, ..., m$, $r_i \in \mathcal{R} \backslash \{r_1\}$, $\lambda \geq 0$ and any two given protection strategies $S' = (r'_{j_1}, ..., r'_{j_m}) \in \overline{\Omega}_K(r_i)$ and $S'' = (r''_{j_1}, ..., r''_{j_m}) \in \overline{\Omega}_K(r_i)$ we have that $L(T, \mathrm{succ}(S'), \lambda) \geq L(T, \mathrm{succ}(S''), \lambda)$ if and only if $L(T, S', \lambda) \geq L(T, S'', \lambda)$.*

**Proof** Let $K \in \{1, ..., m\}$ and $\lambda \geq 0$. For $i = 1, ..., l$ let

$$L_i^T = \lambda R_s(T) + \sum_{k=1}^{K} \left[ D_k^T(r_i) + \lambda n_R \left( \frac{1 - r_i}{r_i} \right) n_k \right].$$

Then, by construction, for $S = (r_{j_1}, ..., r_{j_m}) \in \overline{\Omega}_K(r_i)$,

$$L(T, S, \lambda) = L_i^T + \sum_{k=K+1}^{m} \left[ D_k^T(r_{j_k}) + \lambda n_R \left( \frac{1 - r_{j_k}}{r_{j_k}} \right) n_k \right].$$

Therefore, for $S', S'' \in \overline{\Omega}_K(r_i)$ with $i > 1$ we obtain

$$L(T, \mathrm{succ}(S'), \lambda) = L(T, S', \lambda) - L_i^T + L_{i-1}^T,$$

$$L(T, \mathrm{succ}(S''), \lambda) = L(T, S'', \lambda) - L_i^T + L_{i-1}^T.$$

The proof of the lemma is completed by subtracting these two equations.

For $K = 1, ..., m$ and $i = 1, ..., l$ let us denote by $S_K(r_i)$, $\overline{S}_K(r_i)$ and $L_K(r_i, \lambda)$, $\overline{L}_K(r_i, \lambda)$ optimal protection strategies and corresponding Lagrangian costs,

$$\begin{aligned} S_K(r_i) &= \arg \min_{S \in \Omega_K(r_i)} L(T, S, \lambda), \\ L_K(r_i, \lambda) &= L(T, S_K(r_i), \lambda), \end{aligned}$$

and, correspondingly,

$$\begin{aligned} \overline{S}_K(r_i) &= \arg \min_{S \in \overline{\Omega}_K(r_i)} L(T, S, \lambda), \\ \overline{L}_K(r_i, \lambda) &= L(T, \overline{S}_K(r_i), \lambda). \end{aligned}$$

From the definition of $\overline{\Omega}_K(r_i)$, we conclude that with $k^* = \arg\min_{k=K,...,m} L_k(r_i, \lambda)$ we have

$$\begin{aligned} \overline{S}_K(r_i) &= S_{k^*}(r_i), \\ \overline{L}_K(r_i, \lambda) &= L_{k^*}(r_i, \lambda). \end{aligned}$$

Thus, we can compute an optimal strategy in $\overline{\Omega}_K(r_i)$ from those in $\Omega_K(r_i)$, $i = K, ..., m$.

Using the basic heuristic assumption from above we can obtain the best strategy in $\Omega_K(r_i)$ from that in $\overline{\Omega}_K(r_{i+1})$ simply by replacing the first $K$ rates $r_{i+1}$ by $r_i$, i.e., by taking the successor of $\overline{S}_K(r_{i+1})$.

The algorithm for computing all optimal protection strategies $S_K(r_i)$ and $\overline{S}_K(r_i)$ therefore may proceed in stages $i = l - 1, l - 2, ..., 1$. After initializing the trivial optimal strategies $\overline{S}_K(r_l) = (r_l, ..., r_l)$ for $K = 1, ..., m$ one may write down in stage $i$ strategies $S_K(r_i)$ as $\mathrm{succ}(\overline{S}_K(r_{i+1}))$ and $\overline{S}_K(r_i) = S_{k^*}(r_i)$ with $k^*$ as defined above. Finally, the overall optimal strategy is the best one of $\overline{S}_1(r_i), i = 1, ..., l$. We call this procedure *Algorithm UEP-1*. The pseudo code in Table 2 presents an implementation. The number of evaluations of Lagrangian costs is $m(l - 1) + 1$, which compares favorably with $f(m, l)$.

An alternative to Algorithm UEP-1 was given in [14]. It is based on the assumption in Lemma 3, minimizing $L(T, S, \lambda)$ over arbitrary rate allocations $S \in \mathcal{R}^m$. Thus, with the relation

$$L(T, S, \lambda) = \sum_{k=1}^{m} \left[ D_k^T(r_{j_k}) + \lambda n_R \left( \frac{1 - r_{j_k}}{r_{j_k}} \right) n_k \right] + \lambda R_s(T)$$

the algorithm computes $S = (r_{j_1}, ..., r_{j_m}) \in \mathcal{R}^m$ by

$$r_{j_k} = \arg\min_{r_i \in \mathcal{R}} D_k^T(r_i) + \lambda n_R \left( \frac{1 - r_i}{r_i} \right) n_k$$

for $k = 1, ..., m$. We call this method *Algorithm UEP-2*. (It was named UEP2 in [14].) It requires $ml$ simulations for the evaluation of distortions. Thus, the complexity is similar to that of Algorithm UEP-1.

Algorithms UEP-0, UEP-1, and UEP-2 are designed to minimize $L(T, S, \lambda)$ for fixed $\lambda$ and $T$ over all strategies $S \in \Omega$ as needed in the joint source-channel coding method JSCC-1.

# 4 Results

We consider the fractal coder described in Section 2 as a source coder. The 29 information bits of the range codewords were partitioned in $m = 13$ sensitivity classes (see Table 1).

Our methods for UEP and joint source-channel fractal image coding work independently of the choice of channel coder. For channel coding we used RCPC codes [16] because they are suitable for UEP schemes. Indeed, the same Viterbi decoder can be used for all code rates. The used RCPC coder is given by the convolutional mother code of rate $\frac{1}{N} = \frac{1}{3}$ and memory $M = 6$. Together with $N$, the puncturing period $P = 8$ determines the range of code rates: $R = \frac{p}{p+l}, l = 1, \ldots, (N-1)p$, from which we retained the rates $\frac{8}{24}, \frac{8}{22}, \frac{8}{20}, \frac{8}{18}, \frac{8}{16}, \frac{8}{14}, \frac{8}{12}, \frac{8}{10}, \frac{8}{9}$, and 1. For these rates we experimentally determined the residual bit error rates.

Error-correcting code rates whose residual error probabilities were greater than the BER of the channel were removed. Also, all rates were removed that yielded a zero residual error probability except the highest one of them. Thus, the set of used rates was $\mathcal{R} = \{\frac{8}{24}, \frac{8}{22}, \frac{8}{20}, \frac{8}{18}, \frac{8}{16}, 1\}$ with $l = 6$ for BER $10^{-1}$, and $\mathcal{R} = \{\frac{8}{14}, \frac{8}{12}, \frac{8}{10}, 1\}$ with $l = 4$ for BER $10^{-2}$.

In the first experiment, we considered the $512 \times 512$ Lenna image at source rate of 0.21 bpp and BER of $10^{-1}$. The reconstruction errors were estimated in the optimization using averaged mean square collage error over 50 simulations each. Using the collage error instead of the original reconstruction error

is not a limitation of the method. Many tests showed that when using true reconstruction errors in the optimization the improvements of the resulting source-channel code were less than 0.02 dB of PSNR.

Figure 3 shows the performance of EEP, where for each point the same rate from the total set of 10 retained rates was used for the protection of all bits. This is compared with the performance of the three proposed UEP algorithms UEP-0, UEP-1, and UEP-2. The curve for EEP dips below the PSNR of about 14 dB achieved without error protection (total rate 0.21 bpp) at the first four points corresponding to code rates 8/9, 8/10, 8/12, 8/14. This is explained by the fact that for these code rates the residual bit error rate is higher than the channel BER.

The results show that unequal error protection performed much better than equal error protection. Also, UEP-2 gave worse results than UEP-0 and UEP-1, whereas the difference between UEP-0 and UEP-1 was negligible. Moreover, the CPU time was 8113.6s for UEP-0 and 63.7s for UEP-1. This is in line with our theoretical complexity estimation. For $m = 13$ and $l = 6$ we have to consider $f(m, l) = 8568$ rate allocations in UEP-0, while in UEP-1 the number is $m(l-1)+1 = 66$, which is 0.77% of 8568. This percentage agrees almost exactly with the ratio of our timings. The CPU times were measured on a 270 MHz MIPS R12000 processor of an SGI Origin200 server with main memory size of 1.5 Gbytes. We conclude that the algorithm UEP-1 gave the best performance when considering both PSNR and time. Therefore, in all following tests we used only UEP-1.

Our next experiment showed that the restriction to $m = 13$ classes did not significantly reduce the quality of the error protected codes. Again we set the source rate to 0.21 bpp and used a BER of $10^{-1}$. With the maximum of 29 sensitivity classes only marginally better PSNR values were obtained (Figure 4). Therefore, we continued further experiments only with $m = 13$.

In the previous simulations, the source rate was fixed and the optimal allocation of channel code rates for the data in the $m$ sensitivity classes was searched under the constraint on the channel bit rate. However, joint source-channel coding may enhance the performance of our system. We present results for JSCC-0 and the less complex algorithm JSCC-1 for rate allocation using Lagrangian optimization and UEP-1 as the core algorithm. We used a range of 20 source rates from 0.07 bpp to 0.45 bpp obtained by different quadtree partitions. Thus, the set $\mathcal{T}$ consisted of 20 fractal codes. For Algorithm JSCC-1, convergence occurred already after $k_{\max} = 3$ iterations. Results for the test image Lenna at BER $10^{-1}$ are shown in Figure 5. The reconstruction quality for the codes from the fast algorithm JSCC-1 was only

slightly worse than that of JSCC-0, less than 0.1 dB in PSNR.

For the lower bit error rate $10^{-2}$ the performance gap between JSCC-0 and JSCC-1 was even smaller (see Figure 6). The figure also displays curves for the performance of encodings with fixed source rates from 0.11 to 0.25 bpp. These findings again show the importance of joint source-channel coding as well as the efficiency of our proposed algorithms.

Finally, Figures 7 and 8 present images at different source rates, transmission rates, and bit error rates, with and without joint source-channel coding using unequal error protection.

# 5 Conclusions

We developed and studied a set of algorithms for unequal error protection of fractal image codes in the context of joint source-channel coding. The proposed methods allocate the total transmission rate between the source code and a range of error-correcting codes in a nearly optimal way. We conclude that in practice the combination of our algorithm JSCC-1 with UEP-1 at the core gives the best performance when considering both expected image reconstruction quality and time complexity. Simulations using a quadtree-based fractal encoder and a set of RCPC codes showed that our system is efficient. The results prove that joint source-channel coding with fractal image compression is feasible, leads to efficient protection strategies, and outperforms previous works in this field that only covered channel coding with a fixed source rate.

All the experimental results presented in the paper are for a binary symmetric channel. However, the proposed UEP technique can be used with other channels, including the additive white Gaussian noise channel and the Gilbert-Elliot fading channel. Moreover, our approach is not limited to fractal coders; it can be adapted to other source coders that output fixed length codewords such as some types of vector quantizers.

## Acknowledgments

The support of the German Academic Exchange Service (DAAD) for Y. Charfi is gratefully acknowledged. V. Stanković thanks the Graduiertenkolleg "Wissensrepräsentation" (knowledge representation) of the Deutsche Forschungsgesellschaft (DFG) for funding.

## References


[1] C. E. Shannon, "A mathematical theory of communication," *Bell Syst. Tech. J.*, vol. 27, pp. 379–423 and 623–656, 1948.

[2] A. J. Viterbi and J. K. Omura, *Principles of Digital Communications and Coding*, McGraw-Hill, New York, 1979.

[3] J. W. Modestino and D. G. Daut, "Combined source-channel coding of images," *IEEE Trans. Comm.*, vol. COM-27, pp. 1644–1659, 1979.

[4] J. W. Modestino, D. G. Daut, and A. L. Vickers, "Combined source-channel coding of images using the block cosine Transform," *IEEE Trans. Comm.*, vol. COM-29, pp. 1261–1274, 1981.

[5] B. Hochwald and K. Zeger, "Tradeoff between source and channel coding," *IEEE Trans. Inform. Theory*, vol. IT-43, pp. 1412–1424, 1997.

[6] M. J. Ruf and J. W. Modestino, "Operational rate-distortion performance for joint source and channel coding of images," *IEEE Trans. Image Proc.*, vol. 8, no. 3, pp. 305–320, 1999.

[7] A. J. Goldsmith and M. Effros, "Joint design of fixed-rate source codes and multiresolution channel codes," *IEEE Trans. Comm.*, vol. 46, no. 10, pp. 1301–1312, 1998.

[8] Y. Fisher, *Fractal Image Compression — Theory and Application*, Springer-Verlag, New York, 1994.

[9] D. Saupe and R. Hamzaoui, "The Leipzig Paper Collection on Fractal Image Compression," ftp://shear.informatik.uni-leipzig.de/pub/Fractal/papers/pdf/README.html.

[10] J. Streit and L. Hanzo, "A fractal video communicator," in *Proc. IEEE Veh. Tech. Conf., Stockholm*, 1994, pp. 1030–1034.

[11] G. C. Clark and J. B. Cain, *Error-correction coding for digital communications*, Plenum Press, 1981.

[12] M. Novak, "Transmission error robust fractal coding using a model-residual approach," in *Proc. DCC-98, IEEE Comp. Soc. Press*, 1998, pp. 349–358.

[13] Y. H. Noh, S. H. Kim, and N. C. Kim, "Block loss recovery using fractal extrapolation for fractal coded images," in *Proc. IEEE ICIP-98, Chicago*, 1998.

[14] V. Stanković, R. Hamzaoui, and D. Saupe, "Rate-distortion unequal error protection for fractal image codes," in *Proc. IEEE ICIP-2001, Thessaloniki*, 2001, vol. 1, pp. 98–101.

[15] G. E. Øien and S. Lepsøy, "A class of fractal image coders with fast decoder convergence," in *Fractal Image Compression – Theory and Application*, Y. Fisher, Ed. Springer-Verlag, 1994.

[16] J. Hagenauer, "Rate-compatible punctured convolutional codes (RCPC codes) and their applications," *IEEE Trans. Comm.*, vol. 36,4, pp. 389–400, 1988.

[17] H. Everett, "Generalized Lagrange multiplier method for solving problems of optimum allocation of resources," *Operations Research*, vol. 11, pp. 399–417, 1963.

**Youssef Charfi** was born in Morocco, in 1975. He received the Licence ès Science in Physics and the Diplôme d'études supérieures approfondies (D.E.S.A.) in control, and signal and image processing from Mohammed V University, Rabat, Morocco, in 1997 and 1999, respectively. Since 2000, he has been pursuing the Doctoral degree in joint source-channel coding. From 2001 to 2002, he was a DAAD fellow at the Computer Science Department, University of Leipzig, Leipzig, Germany. He is currently a DAAD fellow at the Computer and Information Science Department, University of Constance, Constance, Germany. His research interests are in image processing and joint source-channel coding.

**Vladimir M. Stanković** was born in Leskovac, Serbia, in 1976. He received the Dipl.-Ing. degree in electrical engineering from the University of Belgrade, Belgrade, Serbia, in 2000. Since 2000 he has been a Ph.D. degree candidate at the Institute of Computer Science, University of Leipzig, Leipzig, Germany, and a DFG (Deutsche Forschungsgemeinschaft) scholarship holder. His research interests include robust image and video transmission over mobile channels and packet networks, error protection coding, and signal processing techniques for digital communications.

**Raouf Hamzaoui** received the Maîtrise de mathématiques from the Faculty of Sciences of Tunis, Tunis, Tunisia, in 1986, the M.Sc. degree in mathematics from the University of Montreal, Montreal, Canada, in 1993, and the Dr. Rer. nat. degree from the Faculty of Applied Sciences of the University of Freiburg, Freiburg, Germany, in 1997. From 1998 to 2002, he was a Research Assistant with the Computer Science Department of the University of Leipzig, Leipzig, Germany. He is currently a Research Assistant with the Department of Computer and Information Science of the University of Constance, Constance, Germany. His research interests include data compression, joint source-channel coding, digital image processing, and numerical methods.

**Ameur Haouari** was born in Morocco, in 1953. He received his first Doctoral degree in signal processing from the University of Mohammed V, Rabat, Morocco, in 1981. He joined the Signal Processing laboratory in the Lausanne Federal Polytechnic Institute (EPFL), Lausanne, Switzerland, as an assistant professor where he initiated a biomedical research project supported by the World Health Organization (WHO). He returned to Morocco in October 1982 as a teaching and research assistant professor in electronics and electrical engineering. He received his second Doctoral degree with honors in 1989 in biomedical engineering. From 1990 to 1996 he was the head of the pattern recognition group engaged on character recognition and image processing systems. Since 1997, he has been the head of the Image Pro-

cessing and Multimedia group (IPMM). He is currently professor in the department of physics, chairman of the Faculty resources center, chairman of the multimedia technical committee, and an active member of the International Association of University Pedagogy (AIPU).

**Dietmar Saupe** received his Dr. rer. nat. and Habilitation degrees, both from the University of Bremen, in 1982 and 1993, respectively. He has served as visiting assistant professor of mathematics at the University of California at Santa Cruz (1985–1987), assistant professor at the University of Bremen (1987–1993), professor of computer science at the Albert-Ludwigs-University of Freiburg (1993–1998), at the University of Leipzig (1998–2002), and at the University of Constance (since 2002). His research has focused on image processing and coding, computer graphics, visualization, and dynamical systems. He is the co-author and editor of several books on fractals, e.g., Chaos and Fractals (Springer-Verlag, New York, 1992). He is a member of the IEEE Signal Processing Society, ACM SIGGRAPH, Eurographics, and others.

# Tables

| sensitivity classes | range codeword bits |
|---|---|
| $C_1$ | $o_6$ |
| $C_2$ | $o_5$ |
| $C_3$ | $o_4$ |
| $C_4$ | $s_4$ |
| $C_5$ | $i_1$ |
| $C_6$ | $i_0, d_4, d_7$ |
| $C_7$ | $d_2, d_3, d_8, d_{10}, d_{11}, d_{12}, d_{13}$ |
| $C_8$ | $i_2, d_5, d_6, d_9$ |
| $C_9$ | $d_1$ |
| $C_{10}$ | $o_3, s_3$ |
| $C_{11}$ | $d_0$ |
| $C_{12}$ | $s_2, o_2$ |
| $C_{13}$ | $s_0, s_1, o_0, o_1$ |

Table 1: Partition of the range codeword bits into 13 sensitivity classes with decreasing sensitivity for a fractal code of the 512 × 512 image Lenna.

*Initialization*
`for` $K := 1, ..., m$ $\quad \overline{S}_K(r_l) := (r_l, ..., r_l)$
*Iteration*
`for` $i := l-1, l-2, ..., 1$
  `for` $K := 1, ..., m$ $\quad$ *// compute* $S_K(r_i)$
    $S_K(r_i) := \mathrm{succ}(\overline{S}_K(r_{i+1}))$
    $L_K(r_i, \lambda) := L(T, S_K(r_i), \lambda)$
  $\overline{S}_m(r_i) := S_m(r_i)$ $\quad$ *// compute* $\overline{S}_K(r_i)$
  $\overline{L}_m(r_i, \lambda) := L_m(r_i, \lambda)$
  `for` $K := m-1, ..., 1$
    $\overline{S}_K(r_i) := S_K(r_i)$
    $\overline{L}_K(r_i, \lambda) := L_K(r_i, \lambda)$
    `if` $L_K(r_i, \lambda) > \overline{L}_{K+1}(r_i, \lambda)$
      $\overline{S}_K(r_i) := \overline{S}_{K+1}(r_i)$
      $\overline{L}_K(r_i, \lambda) := \overline{L}_{K+1}(r_i, \lambda)$
*Result*
$i^* := 1$
`for` $i := 2, ..., l$
  `if` $\overline{L}_1(r_i, \lambda) < \overline{L}_1(r_{i^*}, \lambda)$ $i^* := i$
$S^* := \overline{S}_1(r_{i^*})$ $\quad$ *// optimal strategy*
$L^* := \overline{L}_1(r_{i^*}, \lambda)$ $\quad$ *// minimal Lagrangian cost*

Table 2: Pseudo code of Algorithm UEP-1 for $l$ channel code rates and $m$ sensitivity classes. The algorithm computes an optimal protection strategy for a given code of the fractal transform $T$ and Lagrange parameter $\lambda \geq 0$.

# Figures

Fig. 1. PSNR degradation caused by the corruption of a single range codeword bit with probability $10^{-1}$ separately. The test image was the 512 × 512 Lenna image at source rate 0.21 bpp.

Fig. 2. PSNR vs. BER in all bits of a single fractal parameter for the Lenna image at source rate 0.21 bpp.

Fig. 3. Results for the 512 × 512 Lenna image at source rate 0.21 bpp and BER of $10^{-1}$.

Fig. 4. Comparison of error protection performance at fixed source rate 0.21 bpp, BER $10^{-1}$, and using 13 resp. 29 sensitivity classes.

Fig. 5. Results for the 512 × 512 Lenna image at BER $10^{-1}$. The two curves are for joint source-channel coding.

Fig. 6. Results for the 512 × 512 Lenna image at BER $10^{-2}$. The two top curves are for joint source-channel coding. The four bottom curves are for encodings with fixed source rates and varying channel rates.

Fig. 7. 512 × 512 Lenna image at different source rates $R_s$, transmission rates $R_t$, and bit error rate $10^{-1}$, with and without joint source-channel coding using unequal error protection. The left column images are without error protection ($R_t = R_s$). PSNR results are also given for transmission through a noiseless channel.

Fig. 8. Results as in Figure 7 for BER $10^{-2}$.

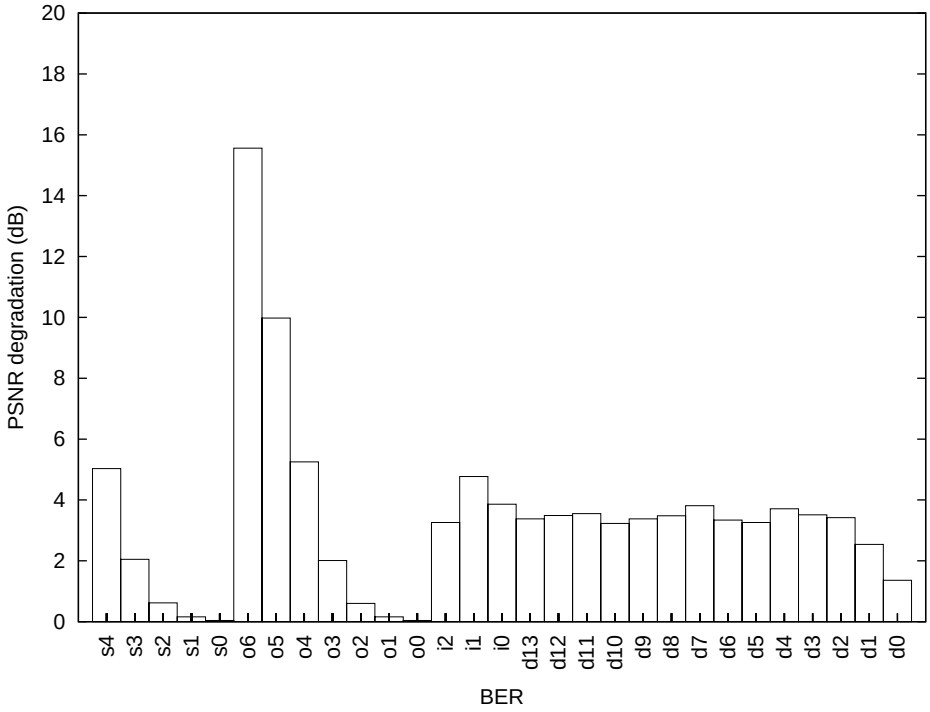
PSNR degradation (dB)
20
18
16
14
12
10
8
6
4
2
0
s4
s3
s2
s1
s0
o6
o5
o4
o3
o2
o1
o0
i2
i1
i0
d13
d12
d11
d10
d9
d8
d7
d6
d5
d4
d3
d2
d1
d0
BER

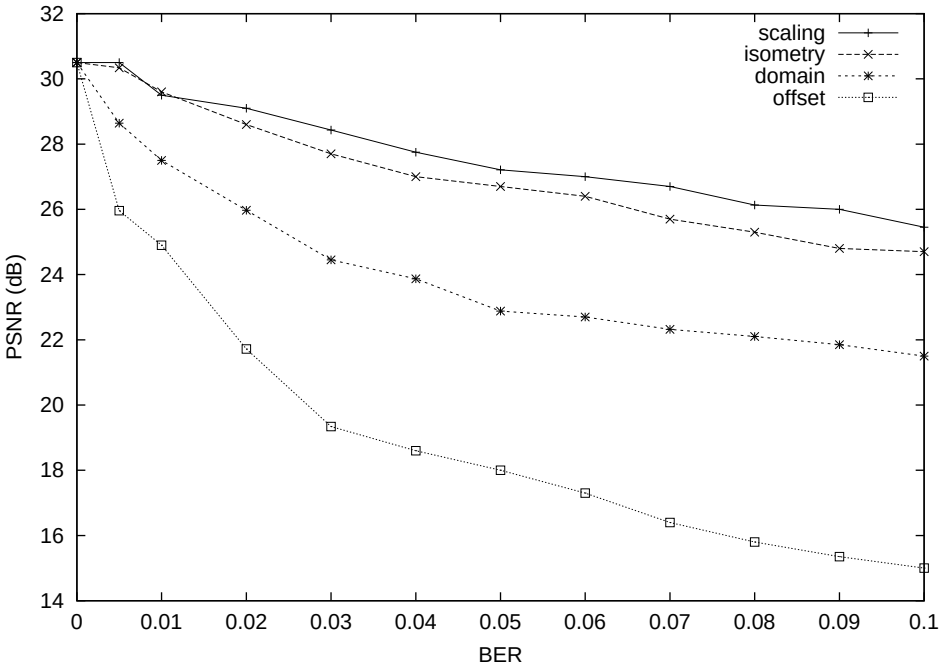
scaling
isometry
domain
offset
PSNR (dB)
BER
32
30
28
26
24
22
20
18
16
14
0
0.01
0.02
0.03
0.04
0.05
0.06
0.07
0.08
0.09
0.1

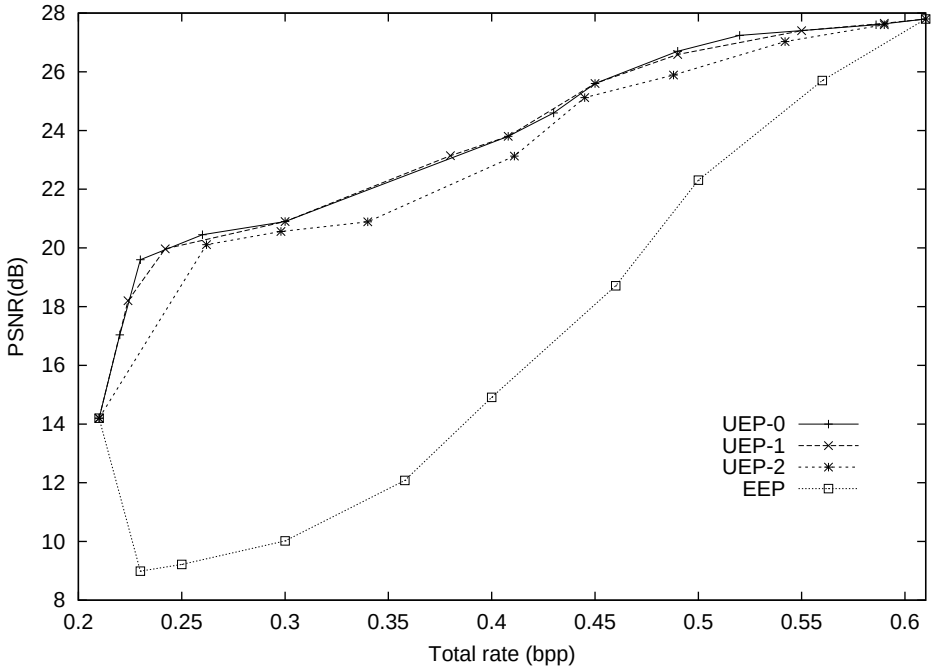
PSNR(dB)
Total rate (bpp)
28
26
24
22
20
18
16
14
12
10
8
0.2
0.25
0.3
0.35
0.4
0.45
0.5
0.55
0.6
UEP-0
UEP-1
UEP-2
EEP

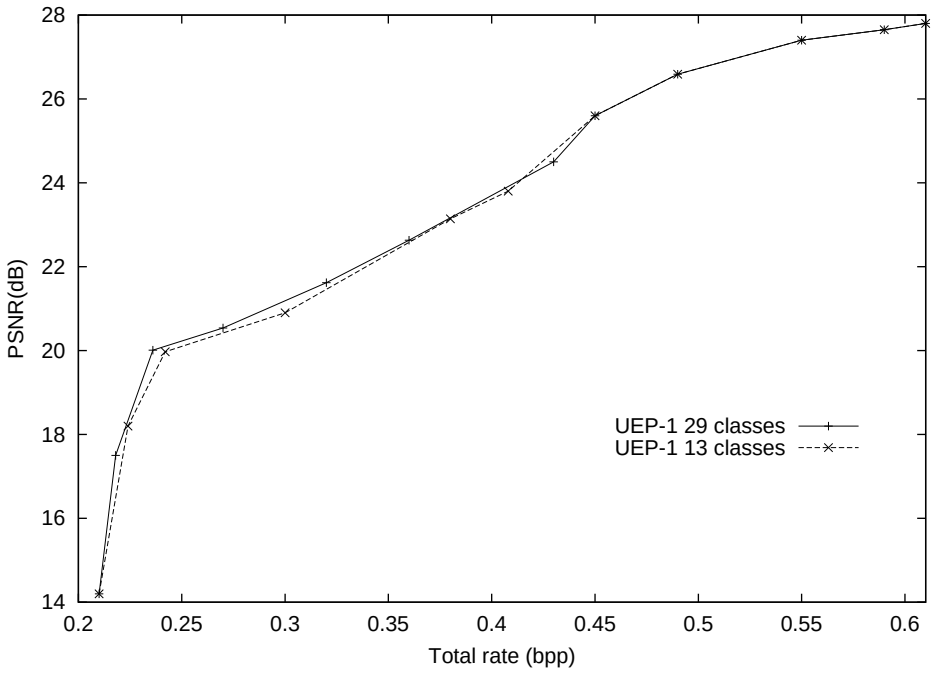
28
26
24
22
20
18
16
14
PSNR(dB)
0.2
0.25
0.3
0.35
0.4
0.45
0.5
0.55
0.6
Total rate (bpp)
UEP-1 29 classes
UEP-1 13 classes

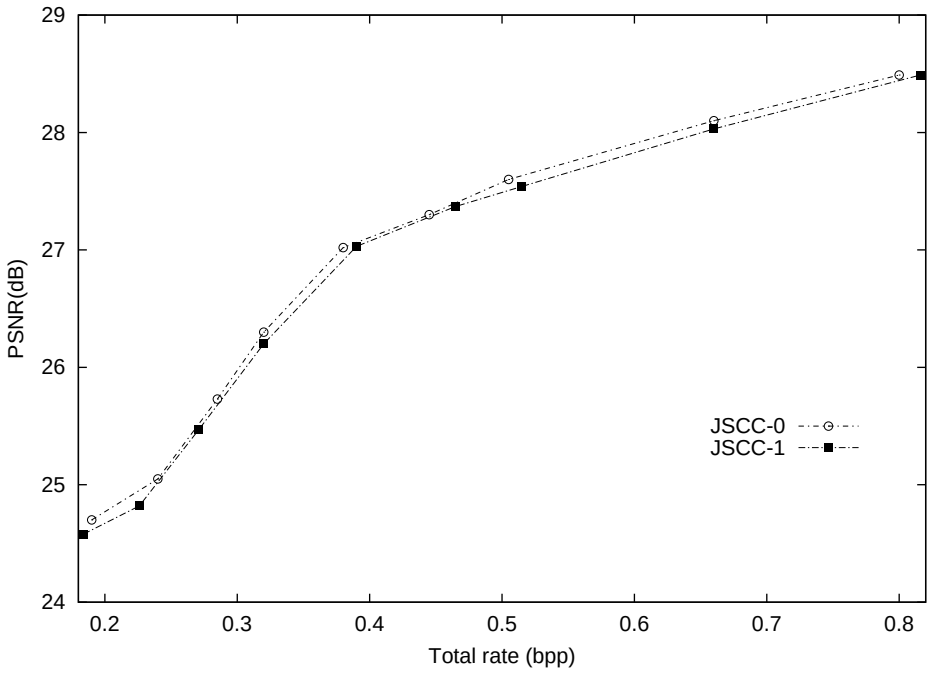
29
28
27
26
25
24
PSNR(dB)
0.2
0.3
0.4
0.5
0.6
0.7
0.8
Total rate (bpp)
JSCC-0
JSCC-1

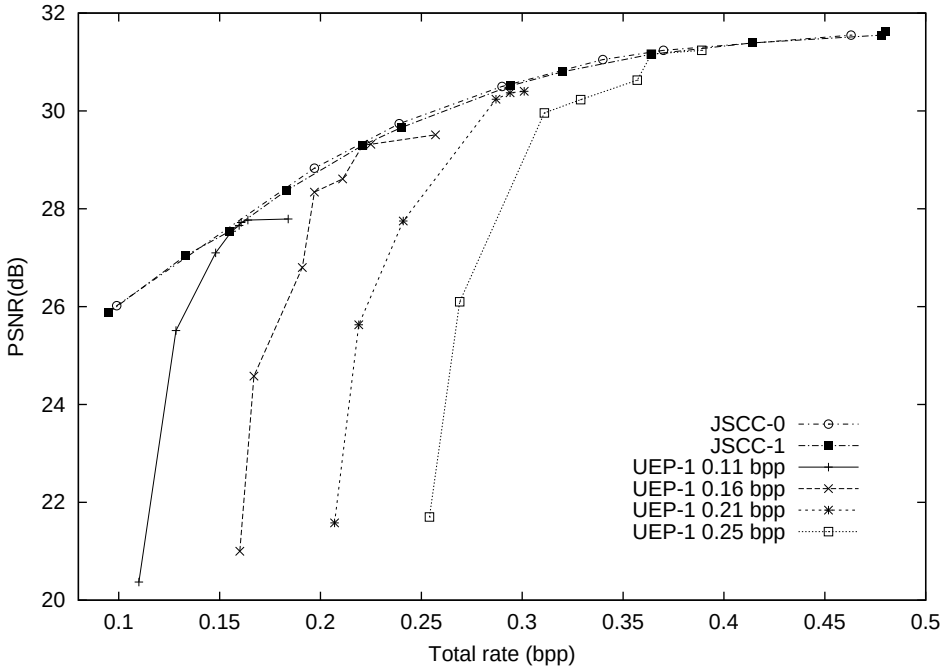
PSNR(dB)
Total rate (bpp)
32
30
28
26
24
22
20
0.1
0.15
0.2
0.25
0.3
0.35
0.4
0.45
0.5
JSCC-0
JSCC-1
UEP-1 0.11 bpp
UEP-1 0.16 bpp
UEP-1 0.21 bpp
UEP-1 0.25 bpp

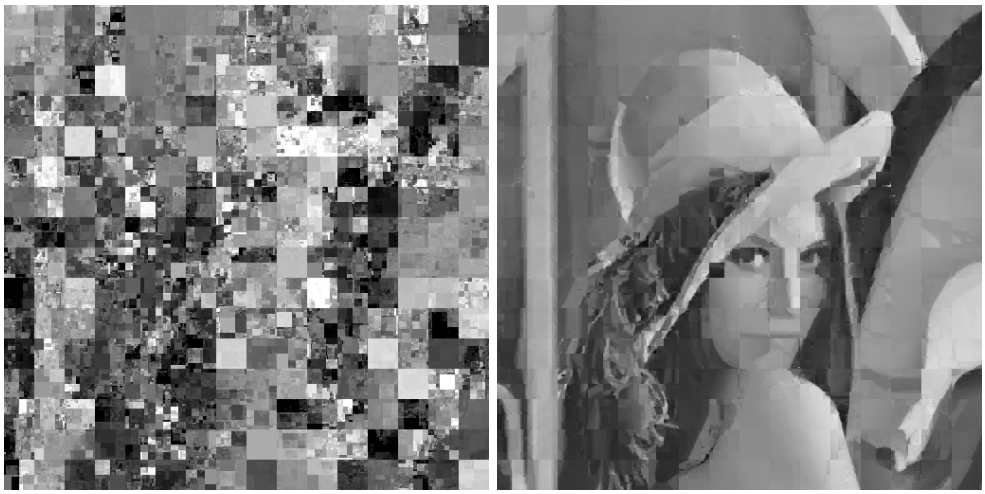

| | left | right | noiseless |
|---|---|---|---|
| BER | 0.10 | 0.10 | 0.00 |
| $R_s$ (bpp) | 0.07 | 0.07 | 0.07 |
| $R_t$ (bpp) | 0.07 | 0.19 | 0.07 |
| PSNR (dB) | 12.82 | 24.70 | 26.07 |

| | left | right | noiseless |
|---|---|---|---|
| BER | 0.10 | 0.10 | 0.00 |
| $R_s$ (bpp) | 0.28 | 0.28 | 0.28 |
| $R_t$ (bpp) | 0.28 | 0.80 | 0.28 |
| PSNR (dB) | 14.11 | 28.49 | 31.43 |

| | left | right | noiseless |
|---|---|---|---|
| BER | 0.01 | 0.01 | 0.00 |
| $R_s$ (bpp) | 0.09 | 0.09 | 0.09 |
| $R_t$ (bpp) | 0.09 | 0.13 | 0.09 |
| PSNR (dB) | 20.11 | 27.04 | 27.16 |

| | left | right | noiseless |
|---|---|---|---|
| BER | 0.01 | 0.01 | 0.00 |
| $R_s$ (bpp) | 0.25 | 0.25 | 0.25 |
| $R_t$ (bpp) | 0.25 | 0.37 | 0.25 |
| PSNR (dB) | 21.56 | 31.24 | 31.29 |